An Explicit Consideration of Desolvation is Critical to Binding Free Energy Calculations of Charged Molecules at Ionic Surfaces

Toshifumi Mori,[†] Robert J. Hamers,[‡] Joel A. Pedersen,[§] and Qiang Cui*,[†]

[†]Department of Chemistry and Theoretical Chemistry Institute, University of Wisconsin—Madison, 1101 University Avenue, Madison, Wisconsin 53706, United States

[‡]Department of Chemistry, University of Wisconsin—Madison, 1101 University Avenue, Madison, Wisconsin 53706, United States

[§]Department of Soil Science, Civil & Environmental Engineering, and Chemistry, University of Wisconsin—Madison, 1525 Observatory Drive, Madison, Wisconsin 53706, United States

S *Supporting Information*

ABSTRACT: Identifying factors that control the strength and specificity of interactions between peptides and nanoparticles is essential for understanding the potential beneficial and deleterious effects of nanoparticles on biological systems. Computer simulations are valuable in this context, although the reliability of such calculations depends on the force field and sampling algorithm, as well as how the binding constant and binding free energy are defined; the latter must be carefully defined with a clear connection to microscopic models based on statistical mechanics. Using the example of formate binding to the rutile titanium dioxide (TiO_2) (110) surface, we demonstrate that a reliable description of the binding process requires an explicit consideration of changes in the solvation state of the binding site. Specifically, we carry out metadynamics simulations in which the solvent coordination number of the binding site, s, is introduced as a collective variable in addition to the vertical distance of the adsorbate to the surface (z). The resulting two-dimensional potential of mean force (2D-PMF) clearly shows that explicitly including the local desolvation of the binding site on the TiO_2 surface strongly impacts the convergence and result of the binding free energy calculations. Projecting the 2D-PMF into a one-dimensional PMF along either z or s leads to large errors in the free energy barriers. Results from metadynamics simulations are quantitatively supported by independent alchemical free energy simulations, in which the solvation state of the binding site is also carefully considered by explicitly introducing water molecules to the binding site as the adsorbate is decoupled from the system. On the other hand, preliminary committor analysis for the approximate transition state ensemble constructed based on the 2D-PMF suggests that to properly describe the binding/unbinding kinetics, variables beyond s and z, such as those describing the hydrogen bonding pattern of the adsorbate and surface water, need to be included. We expect that the insights and computational methodologies established in this work will be generally applicable to the analysis of binding interactions between highly charged adsorbates and ionic surfaces in solution, such as those implicated in peptide/nanoparticle binding and biomineralization processes.
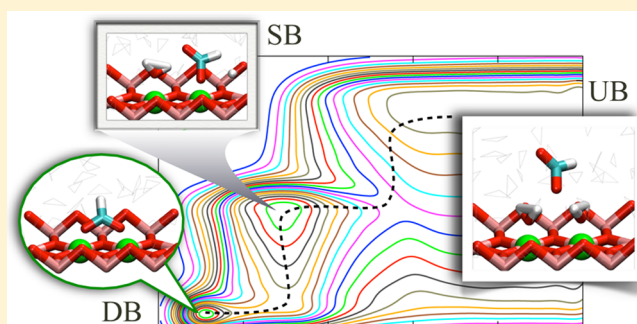
INTRODUCTION

Nanoparticle (NP) based materials have tremendous potential in broad range of technological applications such as solar photovoltaic energy harvesting and conversion, energy storage, catalysis, and drug delivery. On the other hand, concerns exist that NPs may have significant health and environmental impacts due to their interactions with diverse biomolecules.[1−4]

Therefore, it is crucial to understand, at the molecular and physical level, principles that govern the strength and specificity of interactions between NPs and various biomolecules, such as peptides, proteins, nucleic acids, and lipid membranes. The complexity of proteins, such as conformational changes triggered by the binding to NPs, makes it difficult to glean fundamental mechanistic insights.[5−7] Systematic analysis of interaction between small molecules or short peptides and NPs, on the other hand, will help provide insights into sequences/

motifs that preferentially interact with specific NP surfaces as well as the underlying physical origins.[8−17]

Titanium dioxide (TiO_2) is one of the most prevalent nanomaterials owing to its outstanding mechanical and chemical properties.[18] Its surface chemistry driven by photocatalysis is also important for environmental considerations.[19,20] For biomaterials applications, for example, TiO_2 has been used as the material for dental implants due to its resistance to corrosion and biocompatibility.[21,22] The peptide−TiO_2 interface in solution has been explored both experimentally[14−16,23,24] and theoretically.[25−30] Experimental studies have identified several key peptide sequences that favor binding to the TiO_2 surface.[16,31] The importance of electrostatic

interactions has been recognized,[14] although the principles that govern specific interactions with the TiO_2 surface remain poorly understood. Theoretical studies have been conducted via molecular dynamics simulations using classical force fields,[25−28,32] sometimes augmented with quantum mechanical calculations,[26,28,32] to better understand factors that dictate the binding affinity of peptides. These studies highlighted the importance of the water layer on the TiO_2 surface, and both direct and water-mediated TiO_2−peptide binding modes have been discussed for different peptide motifs. For example, Monti and Walsh[25] have studied the potentials of mean force (PMF) for the binding of different amino acid side chain analogs onto rutile TiO_2 (110) surface and demonstrated the relationship between the charged state of the adsorbate and its binding mode.

In essentially all previous theoretical characterization of peptide/TiO_2 binding, the binding affinity was estimated by computing the binding PMF as a function of the vertical distance of the adsorbate to the surface,[25−29] that is, $W(z)$. For most adsorbates, z is expected to be a reasonable order parameter that distinguishes the bound and unbound states; thus, $W(z)$ can, in principle, be used to estimate the binding affinity. In practice, however, computing the one-dimensional $W(z)$ is not always reliable. When the adsorbate is highly charged, its binding to the TiO_2 surface necessarily displaces the surface layer of water molecules. Therefore, a reliable description of the free energy landscape associated with the binding process requires explicitly considering the desolvation process as part of the reaction coordinate. In other words, since water molecules bind tightly to TiO_2, changing z alone is insufficient to induce reversible changes in solvation and therefore leads to sampling errors. Indeed, previous studies often found sharply varying PMFs as functions of z,[25,28] indicating that there are important orthogonal degrees of freedom that have not been sampled adequately. Although this is expected to be most serious to the description of the barrier region, insufficient sampling of the desolvation process will also propagate into large statistical errors for the bound state of the computed PMF.

In this work, to overcome this sampling problem, we explicitly introduce a collective coordinate (s) to account for the change of the solvent coordination number of the Ti atoms that form the binding site. Specifically, we characterize the binding process with a two-dimensional PMF, $W(z,s)$, which is computed with metadynamics. We illustrate the protocol by studying the binding of a formate anion (HCOO−) to the TiO_2 surface. To further demonstrate the reliability of the protocol, we compute the binding affinity with an alchemical free energy perturbation approach, which, to the best of our knowledge, has not been applied to adsorbate−surface binding problems. We also carry out a preliminary analysis for the kinetic bottleneck for the binding/unbinding process by examining the committor distribution for the approximate transition state ensemble constructed based on the 2D-PMF. We expect that these computational methodologies will be particularly valuable to the analysis of binding interactions between highly charged adsorbates and highly charged surfaces, such as those implicated in peptide/NP binding and biomineralization processes.[33]

■ COMPUTATIONAL METHODS

System Setup. Although most TiO_2 nanocrystals are in the anatase form, we study here the rutile form (110) surface because we expect the issue of considering a solvation coordinate for interfacial binding is general; the (110) surface is the lowest-energy face of rutile TiO_2 and is electrically neutral. The TiO_2 system is prepared by replicating the unit cell to create a 6-layer slab with a dimension of roughly $29.6 \times 32.5 \times 19.5$ Å^3. The slab consists of 600 titanium and 1200 oxygen atoms, and the top and bottom surfaces ((x,y) plane) are interfaced to water. One formate anion (HCOO−), one sodium cation (Na+) (to ensure charge neutrality), and 2235 water molecules are then added to set up a system in a $33.11 \times 35.54 \times 109.55$ Å^3 box.

Titanium and oxygen atoms in TiO_2 are constrained in space to the crystal structure positions using a harmonic potential with a large force constant of 1000.0 kcal·mol−1·Å−2. The van der Waals (vdW) and charge parameters for TiO_2 are taken from refs 26 and 34. Water molecules are treated with the TIP3P model,[35] and the formate anion is described with the AMBER ff99 force field and AM1-BCC charges[36,37] (see Supporting Information).

Periodic boundary condition is imposed. The long-range electrostatic interactions are treated with the particle mesh Ewald (PME) method[38] with a FFT grid of $30 \times 32 \times 90$ and a real-space cutoff at 10 Å, and van der Waals interactions are cutoff at 10 Å. Bonds involving hydrogen are constrained with the SHAKE algorithm.[39] Equilibration simulation is carried out with the NPT (300 K, 1 atm) ensemble for 200 ps, after which the box size is shrunk to $28.90 \times 31.32 \times 90.93$ Å^3. Subsequent calculations are performed under the constant-NVT (300 K) condition with a time step of 2 fs (unless otherwise specified), and the temperature is maintained with the Langevin thermostat using a collision frequency of 1.0 ps−1. All MD simulations are performed using the AMBER 12 or 11 program packages;[40] for metadynamics, AMBER is interfaced with the PLUMED package.[41]

Binding Free Energy. Consider the binding equilibrium that involves ligand **L**, nanoparticle **NP**, and complex **NP·L**: **L** + **NP** ⇌ **NP· L**. To define an equilibrium constant and binding free energy that can be rigorously connected to both experimental measurements and microscopic models, one has to carefully treat issues related to the standard state[42−44] and the number of ligands that can bind to each nanoparticle.[45] In this work, we focus on the issue of sampling and comparison of two independent simulation approaches (PMF vs alchemical free energy perturbation); thus, we take the simplifying condition that each nanoparticle binds up to only *one* ligand, which is the infinite dilute limit of the binding equilibrium. With this approximation, the equilibrium binding constant (K_b) and standard binding free energy ($\Delta G^\circ_{binding}$) can be defined in a similar fashion as those for protein−ligand binding,[42−44] that is, $K_b = [NP·L]/[NP][L]$ and $\Delta G^\circ_{binding} = -k_B T \ln(C^\circ K_b)$, where C° is a standard concentration (1/1660 Å−3).

The microscopic expressions of K_b and $\Delta G^\circ_{binding}$ are given by the ratios of relevant configuration integrals,[42−44]

$$K_b = \frac{1}{C^\circ} e^{-\beta \Delta G^\circ_{binding}} = \frac{\int_{bd} d\mathbf{R}_u \int d\mathbf{X}\, e^{-\beta u_{tot}}}{\int_{unb} d\mathbf{R}_u \int d\mathbf{X}\, \delta(\mathbf{R}_u - \mathbf{R}^*_u) e^{-\beta u_{tot}}}$$

$$= \frac{\int_{bd} d\mathbf{R}_u \int d\mathbf{X}\, e^{-\beta u_{tot}}}{\int_{bd}^{1,2} d\mathbf{R}_u \int d\mathbf{X} e^{-\beta u_{tot}}}$$

$$\times \frac{\int_{bd}^{1,2} d\mathbf{R}_u \int d\mathbf{X} e^{-\beta u_{tot}}}{\int_{unb} d\mathbf{R}_u \int d\mathbf{X}\, \delta(\mathbf{R}_u - \mathbf{R}^*_u)\, e^{-\beta u_{tot}}} = N_{pair} K_b'$$

$$= N_{pair} \frac{1}{C^\circ} e^{-\beta \Delta G^{1,2}_{binding}} \tag{1}$$

Here, $\beta = 1/(k_B T)$, $\mathbf{R}_u$, and $\mathbf{X}$ are the Cartesian coordinates of the ligand (HCOO$^-$ in this study) and the remaining atoms, respectively, and u_{tot} is the total potential energy of the system. Subscripts "bd" and "unb" denote the bound and unbound regions, respectively. The superscript "1,2" indicates that only the binding to a specific pair of surface Ti atoms (Ti1 and Ti2) is considered in the microscopic simulation, and N_{pair} accounts for the fact that there are many degenerate binding sites on each nanoparticle. $\mathbf{R}^*_u$ is the position of ligand in bulk far apart from the surface of the nanoparticle. In the following, we focus on the site-specific quantity $\Delta G^{1,2}_{binding}$.

In the current study, $\Delta G^{1,2}_{binding}$ is obtained using two independent approaches. In the first approach, we integrate the potential of mean force (PMF)[44] obtained from metadynamics simulations;[46]

$$e^{-\beta \Delta G^{1,2}_{binding}} = e^{\beta \Delta G^{bd}_{tube}} e^{-\beta \Delta G^{PMF}_{binding}} e^{-\beta \Delta G^{unb}_{tube}} \tag{2}$$

where

$$e^{-\beta \Delta G^{bd}_{tube}} = \frac{\int_{bd}^{1,2} d\mathbf{R}_u \int d\mathbf{X}\, e^{-\beta(u_{tot}+u_{tube})}}{\int_{bd}^{1,2} d\mathbf{R}_u \int d\mathbf{X}\, e^{-\beta u_{tot}}} \tag{3}$$

$$e^{-\beta \Delta G^{PMF}_{binding}} = \frac{\{C^\circ\}^{1/3} \int_{bd}^{1,2} d\mathbf{R}_u \int d\mathbf{X}\, e^{-\beta(u_{tot}+u_{tube})}}{\int_{unb} d\mathbf{R}_u \int d\mathbf{X} \delta(\mathbf{R}_u - \mathbf{R}^*_u)_z e^{-\beta(u_{tot}+u_{tube})}}$$

$$= \{\{C^\circ\}^{1/3} \int_{bd}^{1,2} d\mathbf{R}_u \int d\mathbf{X} \int dz' \int ds' \delta(z[\mathbf{R}_u, \mathbf{X}] - z')$$

$$\delta(s[\mathbf{R}_u, \mathbf{X}] - s') e^{-\beta(u_{tot}+u_{tube})}\} / \{\int_{unb} d\mathbf{R}_u \int d\mathbf{X} \int dz'$$

$$\int ds' \delta(z[\mathbf{R}_u, \mathbf{X}] - z') \delta(s[\mathbf{R}_u, \mathbf{X}] - s') \delta(\mathbf{R}_u - \mathbf{R}^*_u)_z e^{-\beta(u_{tot}+u_{tube})}\}$$

$$= \frac{\{C^\circ\}^{1/3} \int_{bd}^{1,2} dz \int ds\, e^{-\beta W(z,s)}}{\int_{unb} dz \int ds \delta(z - z^*) e^{-\beta W(z,s)}} \tag{4}$$

$$e^{-\beta \Delta G^{unb}_{tube}} = \{C^\circ\}^{2/3} \frac{\int_{unb} d\mathbf{R}_u \int d\mathbf{X} \delta(\mathbf{R}_u - \mathbf{R}^*_u)_z e^{-\beta(u_{tot}+u_{tube})}}{\int_{unb} d\mathbf{R}_u \int d\mathbf{X} \delta(\mathbf{R}_u - \mathbf{R}^*_u) e^{-\beta u_{tot}}} \tag{5}$$

Here, u_{tube} is a tube-like restraining potential to ensure that HCOO$^-$ approaches Ti1 and Ti2 during the metadynamics simulation; its effect is removed formally by considering ΔG^{bd}_{tube} and ΔG^{unb}_{tube} (see Results and Discussion). $\delta(\cdots)_i$ for $i = \{x,y,z\}$ denotes the ith component of the Dirac delta function. z and s are the reaction (collective) coordinates in the metadynamics simulations that specify the vertical distance of HCOO$^-$ to the surface and the level of solvation for the surface binding site, respectively, and $z^* = z[\mathbf{R}^*_u, \mathbf{X}]$. The precise expressions of u_{tube}, z, s are given in the next section that summarizes technical details of the metadynamics simulations. $W(z, s)$ in eq 4 is the two-dimensional PMF,

$$e^{-\beta W(z',s')} \propto \int d\mathbf{R}_u \int d\mathbf{X}\, \delta(z[\mathbf{R}_u, \mathbf{X}] - z')$$

$$\delta(s[\mathbf{R}_u, \mathbf{X}] - s') e^{-\beta(u_{tot}+u_{tube})} \tag{6}$$

In the second approach, we use the alchemical free energy perturbation (FEP) method,[43,47] which is widely used to study binding in the biomolecular simulation community. Briefly, using the concept of thermodynamic cycle, $\Delta G^{1,2}_{binding}$ is written as

$$e^{-\beta \Delta G^{1,2}_{binding}} = e^{\beta \Delta G^{bd}_{trans}} e^{\beta \Delta G^{bd}_{uncouple}} e^{-\beta \Delta G^{unb}_{trans}} e^{-\beta \Delta G^{unb}_{uncouple}} \tag{7}$$

where $\Delta G^{bd}_{uncouple}$ and $\Delta G^{unb}_{uncouple}$ are the free energies required to uncouple HCOO$^-$ from the system in the bound and unbound states, respectively; ΔG^{unb}_{trans} and ΔG^{bd}_{trans} are the free energy components associated with the positional restraints applied to unbound species prior to the alchemical perturbations.[43] For more details, see the following text.

Metadynamics. Metadynamics simulations[46] are performed to calculate the PMF of HCOO$^-$ binding/unbinding to the rutile TiO$_2$ (110) surface. Two reaction coordinates, the distance between HCOO$^-$ and TiO$_2$ surface along the z direction and the solvent coordination number[48] of the binding site (Ti1 and Ti2 atoms), are defined as

$$z = z_{OM} - z_{TiM} \tag{8}$$

and

$$s = \sum_{i \in \{Ti1,Ti2\}} \sum_{j \in O_{solvent}} s_{ij} \tag{9}$$

Here, z_i is the z coordinate of atom i, OM and TiM are the centers of the two O atoms in HCOO$^-$ (O1 and O2) and Ti1 and Ti2, respectively, and

$$s_{ij} = \begin{cases} 1 & \text{if } r_{ij} \leq d_0 \\ \dfrac{1 - \{(r_{ij} - d_0)/r_0\}^6}{1 - \{(r_{ij} - d_0)/r_0\}^{12}} & \text{if } r_{ij} > d_0 \end{cases} \tag{10}$$

where r_{ij} is the distance between atoms i and j and d_0, r_0 is set to 0.50 and 1.50 Å, respectively. To ensure that HCOO$^-$ stays above Ti1 and Ti2, a "tube" restraint, u_{tube}, is applied,

$$u_{tube} = \begin{cases} 0 & \text{if } d_{OM-TiM} \leq d_{tube} \\ k_{tube}(d_{OM-TiM} - d_{tube})^2 & \text{if } d_{OM-TiM} > d_{tube} \end{cases} \tag{11}$$

Here, d_{OM-TiM} is the distance between the centers OM and TiM projected on the (x, y) plane and the force constant k_{tube} and the tube radius d_{tube} are set to 200.0 kcal·mol^{-1}·Å^{-2} and 1.50 Å, respectively. As mentioned above, the effect of the tube restraint on the binding free energy is formally removed by considering ΔG^{bd}_{tube} and ΔG^{unb}_{tube} (see Results and Discussion).

The PLUMED package[41] interfaced to AMBER 11 is used to run two sets of metadynamics simulations. To adequately describe the behavior of the system when the formate anion is close to the surface, two-dimensional (2D) (z and s) metadynamics calculations are carried out with a restraint of $z \leq 6.0$. To describe the situation where the formate anion is relatively far from the surface, one-dimensional (1D) (z) metadynamics calculations are carried out with a restraint of 4.0
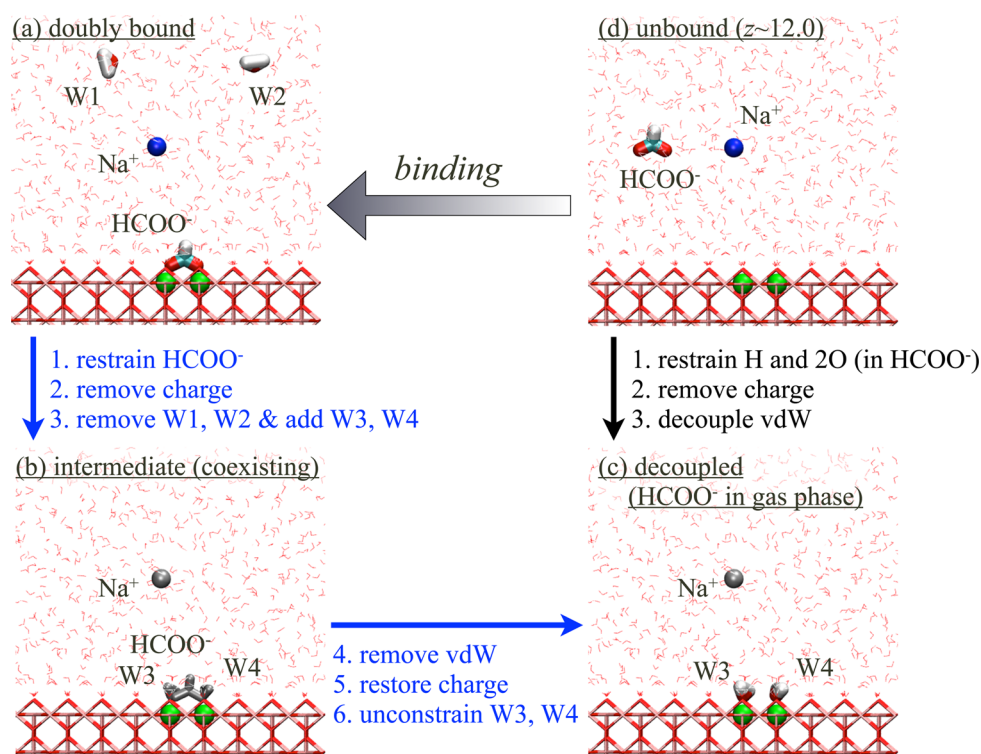
Figure 1. Scheme of alchemical transformation steps used to compute the site-specific binding affinity of formate to a TiO$_2$ surface. The transformation from the bound and unbound states proceed through the following: (a) HCOO$^-$ doubly bound state → (b) uncharged HCOO$^-$, W3, and W4 bound intermediate state → (c) HCOO$^-$ decoupled state (i.e., HCOO$^-$ transferred to the gas phase), and (d) HCOO$^-$ unbound state → (c), respectively. The key waters (W1, W2 removed from bulk and W3, W4 introduced to the binding site in step a → b), TiO$_2$, and HCOO$^-$ are in the licorice representation, and bulk water is shown in lines. The two key Ti atoms (Ti1 and Ti2), Na$^+$, oxygen, carbon, and hydrogen are colored in green, blue, red, cyan, and white, respectively, while grayed spheres represent atoms without charge. Note that unbound species (e.g., Na$^+$ and HCOO$^-$ in d) are also subject to a set of λ-independent positional restraints throughout the FEP simulations and the effects of those restraints are evaluated analytically (see text).

$\leq z \leq 15.0$; when HCOO$^-$ is sufficiently far from the TiO$_2$ surface, the solvent coordinate (s) is not expected to be as critical (*vide infra*). The well-tempered metadynamics method[49] is utilized with a bias factor of 10 and 50 for the 1D and 2D calculations, respectively. The initial Gaussian height is set to 0.1 kcal·mol^{-1}, and the Gaussian width for z and s coordinates are set to 0.2 Å and 0.1, respectively. A new Gaussian potential is added every 1 ps during the simulation. The boundary on z is set by applying a half-harmonic restraint with a force constant of 250 kcal·mol^{-1}·Å^{-2}, that is, a harmonic potential along z that applies only when z exceeds the boundary. The 1D and 2D simulations are ran for 110 and 150 ns, respectively.

Alchemical Free Energy Perturbation. The alchemical FEP calculations[43,47] are performed to calculate the free energies required to uncouple HCOO$^-$ from the unbound and the doubly bound (i.e., with both oxygens attached to the TiO$_2$ surface, see Figure 1) states, respectively. To preserve the charge neutrality of the system during the uncoupling process, the charge on a Na$^+$ in the bulk is also removed whenever the charges on the formate anion are perturbed; this helps remove potential artifacts associated with PME for systems with a net charge.[50−52] Moreover, care is exercised to consider the solvation state of the binding site as HCOO$^-$ is decoupled in the bound state by explicitly removing two water molecules from the bulk (W1, W2) and reintroducing them (W3, W4) to the binding site. Accordingly, the alchemical FEP calculations involve multiple steps as summarized in Figure 1. As described

in previous work,[43] for all unbound species under perturbation (i.e., Na$^+$ and HCOO$^-$ in the unbound state alchemical simulations and Na$^+$, W1, and W2 in the bound state alchemical simulations), a positional restraint (one atom per species) is introduced throughout (i.e., λ-independent) the alchemical perturbations to improve the convergence of FEP calculations;[43,47] the effects of those restraining potentials, $\Delta G_{\text{trans}}^{\text{bd}}$ and $\Delta G_{\text{trans}}^{\text{unb}}$, are considered with analytical expressions discussed below. In addition to those single-atom positional restraints on unbound species, harmonic restraints are also introduced to bound species (e.g., HCOO$^-$ and W3, W4 in the bound state) as part of the alchemical FEP cycles to further control the convergence of such calculations; these λ-dependent positional restraints are applied and removed to ensure that FEP calculations for the bound and unbound states converge to identical system configurations to complete the thermodynamic cycle.

More specifically, for the unbound state (with HCOO$^-$ placed away from the surface by about 12 Å in the z direction), the uncoupling process involves (Figure 1d → c): (1) turn on harmonic restraints on the H and O atoms in HCOO$^-$, (2) remove the charges on HCOO$^-$ and Na$^+$, (3) remove HCOO$^-$ vdW interactions with the rest of the system. Note that after the last step the charge on Na$^+$ is set to zero but it maintains vdW interactions with other atoms. For the bound state, on the other hand, six steps are taken to smoothly decouple HCOO$^-$ on the surface while simultaneously attaching two water molecules to the surface (Figure 1a → b → c): (1) turn on harmonic

restraints on all the atoms in $HCOO^-$, (2) remove charges on $HCOO^-$, Na^+, W1, and W2, (3) remove vdW interactions associated with W1 and W2 but simultaneously introduce two uncharged waters (W3 and W4) right above Ti1 and Ti2 with harmonic restraints, (4) remove $HCOO^-$ vdW interactions with the rest of the system, (5) restore charges on W3 and W4, and (6) remove the harmonic restraints on W3 and W4. In the intermediate state (Figure 1c), both W3−W4 and $HCOO^-$ interact with the TiO_2 surface but they do not interact with each other. Also note that the symmetry numbers from the binding pattern of $HCOO^-$ and W3−W4 cancel out and thus do not appear in the final expression of the binding free energy. Both unbound- and bound-state alchemical simulations lead to the same state (Figure 1c) to complete the thermodynamic cycle: $HCOO^-$ is decoupled from the system and becomes a chargeless molecule harmonically restrained in space without any intermolecular interactions.

To remove the effects of the λ-independent positional restraints on unbound species that are applied throughout the alchemical perturbations, the following approximate analytical expressions are used,

$$e^{-\beta\Delta G_{trans}^{bd}} = \frac{\int_{bd}^{1,2} d\mathbf{R}_u \int d\mathbf{X}\, e^{-\beta(u_{tot}+u_{trans}^{bd})}}{\int_{bd}^{1,2} d\mathbf{R}_u \int d\mathbf{X}\, e^{-\beta u_{tot}}} \tag{12}$$

$$\simeq \frac{N_{WAT}^{unb}(N_{WAT}^{unb}-1)}{2} \prod_{i}^{\{W1,W2,Na^+\}} \left\{ \frac{1}{V_{unb}} \int_{unb} d\mathbf{R}_i\, e^{-\beta u_{trans}^i} \right\} \tag{13}$$

$$e^{-\beta\Delta G_{trans}^{unb}} = C^\circ \frac{\int_{unb} d\mathbf{R}_u \int d\mathbf{X}\, e^{-\beta(u_{tot}+u_{trans}^{unb})}}{\int_{unb} d\mathbf{R}_u \int d\mathbf{X}\, \delta(\mathbf{R}_u - \mathbf{R}_u^*)e^{-\beta u_{tot}}} \tag{14}$$

$$\simeq \frac{C^\circ}{V_{unb}} \prod_{i}^{\{Na^+,HCOO^-\}} \int_{unb} d\mathbf{R}_i\, e^{-\beta u_{trans}^i} \tag{15}$$

Here, $u_{trans}^{bd} = u_{trans}^{W1} + u_{trans}^{w2} + u_{trans}^{Na^+}$ and $u_{trans}^{unb} = u_{trans}^{HCOO^-} + u_{trans}^{Na^+}$ with u_{trans}^i being the positional restraint on one of the atoms in each species i (with a force constant of 1000.0 kcal·mol^{-1}·Å^{-2}). N_{WAT}^{unb} is the number of water molecules in the unbound region (which is 2137 in the current work when $HCOO^-$ is bound to the surface). $V_{unb}(= \int_{unb} d\mathbf{R})$ is the volume of the unbound region, and u_{tot} is approximated to be constant in the unbound region. Note that the Na^+ terms in eqs 13 and 15 cancel out, and for the water terms, we use the box volume instead of C° as we intend to compare the alchemical FEP and metadynamics results.

Soft-core potential[53,54] is used when vdW interaction is perturbed, and λ values in the perturbation are taken to be [0.05,0.95] for vdW interaction and [0.0,1.0] otherwise with an increment of 0.10. For the restraining step of unbound $HCOO^-$, the region of $0.0 \leq \lambda \leq 0.1$ is further sampled with an increment of 0.01 to improve the overlap between different λ windows. The Bennett acceptance ratio (BAR) method[47,55] is used to calculate the free energy difference, and end points are linearly extrapolated when needed. Each λ window is ran for 2 ns while storing the potential information every 1 ps. First 500 ps is considered as the equilibration, and the last 1.5 ns is used for production.

Committor Analysis for the Approximate Transition State Ensemble. To further understand whether s and z are

sufficient to characterize the kinetic bottleneck for the adsorbate binding/unbinding process, we perform committor analysis[56,57] for the approximate transition state ensemble collected based on the 2D(s,z)-PMF. Since it is not straightforward to apply a holonomic constraint on the collective coordinates used in the current study, and metadynamics simulations of ~100 ns scale have limited resolution on the precise location of the saddle point on the computed 2D-PMF, we first select two approximate transition state configurations from the computed 2D-PMF ($(z, s) =$ (3.75, 0.99) and (3.77, 0.99), hereafter denoted as TS1 and TS2, respectively). Using each configuration as the reference and a harmonic constraint with a force constant of 10 000 kcal·mol^{-1}·Å^{-2}, 100 additional configurations are collected using MD simulations at 300 K and trajectories of length 10 ps. Starting from each of the 200 configurations that form the approximate transition state ensemble, 100 NVE trajectories (with a time step of 1 fs) are carried out starting with random velocities drawn from the Gaussian distribution at 300 K; each trajectory is propagated both forward and backward in time for ~1 ps in each direction, from which the committor distribution is calculated.

■ RESULTS AND DISCUSSION

Metadynamics Simulations. We first examine the metadynamics result to better understand the binding/unbinding processes. The time evolution of the collective coordinates z and s from the two-dimensional metadynamics trajectory is shown in Figure 2. The figure shows that the
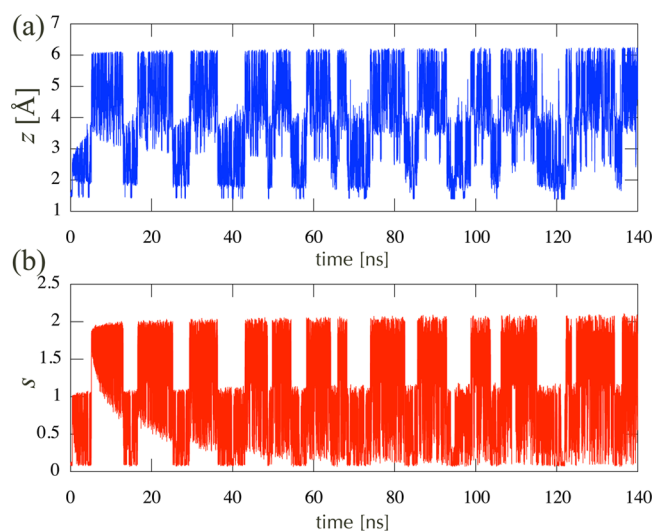

Figure 2. Time evolution of the reaction (collective) coordinates (a) z and (b) s in the two-dimensional metadynamics simulation.

sampling sufficiently covers the phase space of interest and indicates the existence of three states, which can be characterized by (1) $z \simeq 1.5$ and $s \simeq 0.1$, (2) $1.8 \leq z \leq 3.8$ and $0.1 \leq s \leq 1.0$, and (3) $3.0 \leq z(\leq 6.0)$ and $0.8 \leq s \leq 2.0$, respectively. These three states have different $HCOO^-$-TiO_2 interaction patterns and are hereafter denoted as the doubly bound (DB), singly bound (SB), and unbound (UB) states, respectively (for representative snapshots, see Figure 4).

The 2D potential of mean force (2D-PMF) is constructed by gathering the Gaussian bias potentials obtained from the metadynamics trajectory and shown in Figure 3. The three
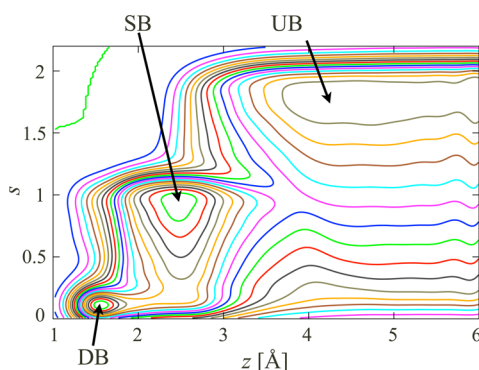
Figure 3. Two dimensional potential of mean force constructed from the two-dimensional metadynamics simulation. Contour line is drawn every 5 kcal/mol. DB, SB, and UB represent the doubly bound, singly bound, and unbound minima, respectively.
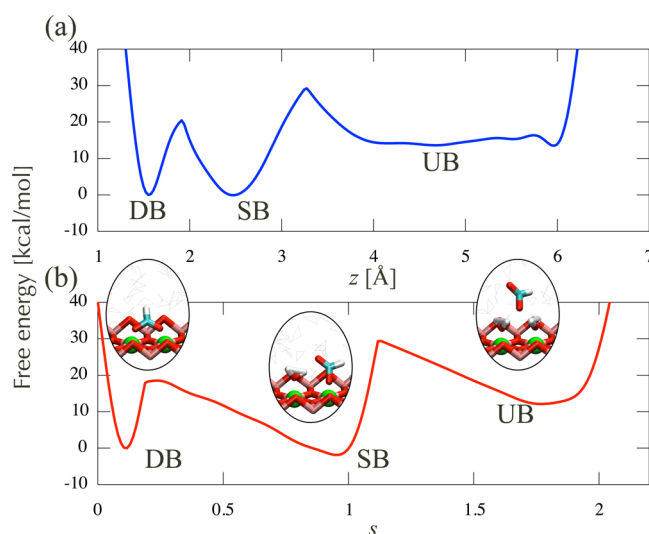

Figure 4. One dimensional potentials of mean force along (a) z and (b) s coordinates, constructed from the two-dimensional PMF in Figure 3 by integrating the other coordinate. Representative snapshots for the DB, SB, and UB state minima are shown as insets. The energies are measured from the DB minima in each plot. Note that the free energy minima at around $z = 6.0$ in (a) is an artifact due to the wall potential set at $z = 6.0$ Å.[41] We neglected this part in considering the UB minimum in z space, but it is included in the UB state in the s space.

states can be clearly distinguished in this figure, and the free energies of the SB and UB state minima (measured relative to the DB state minimum) are estimated to be 0.5 and 14.5 kcal/mol, respectively. The transition states (TSs) between DB and SB states, SB and UB states are found to be 23.0 and 41.2 kcal/mol relative to the DB state minimum. The PMF explicitly indicates that in the binding process, a pronounced decrease in the solvent coordinate s (i.e., desolvation of Ti1 and Ti2) occurs prior to the TS; this is followed by a sudden decrease in the binding distance z (HCOO⁻ binding) once the TS is passed. Thus, the binding is driven by desolvation, which emphasizes the need to explicitly sample the solvent coordinate to construct a continuous PMF for the binding process. On the other hand, in the dissociation process, z elongation is the dominant change prior to the TS, thus the z coordinate needs to be adequately sampled as well. This asymmetry in key coordinate for the binding and unbinding processes is further illustrated by projecting the 2D-PMF into the z and s spaces by integrating over one of the coordinates; the resulting 1D-PMFs as functions of z and s, respectively, are plotted in Figure 4. Figure 4(a) and (b) show that while the free energies of the SB and UB state minima (measured relative to the DB minimum) are fairly consistent with the 2D PMF (−0.1 and 13.6 kcal/mol in z and −1.9 and 12.1 kcal/mol in s, respectively, as compared to 0.5 and 14.5 kcal/mol in the 2D PMF), the free energy barriers between different minima are significantly underestimated (20.4 and 29.2 in z and 18.5 and 29.4 kcal/mol in s, as compared to 23.0 and 41.2 kcal/mol from the 2D PMF). These discrepancies are due to the overlap of the distribution tails of the three states when the 2D PMF is integrated either along the z or s coordinate,[48] and they highlight the need to consider both z and s coordinates in constructing a reliable potential of mean force, especially for the barrier regions. Note that a similar issue associated with projecting the PMF to lower dimensions has also been discussed in solution[57] and protein simulations.[58]

The PMF that covers larger z values (for the range $4 \leq z \leq 15$) is further explored with a 1D metadynamics simulation (including the tube constraint). Note that the desolvation effect can be safely omitted when $z \geq 4.0$ Å (see Figure 3). The result is given in Figure 5a, together with the 1D PMF constructed from the 2D metadynamics (Figure 4a) as reference. Apart from the artificial energy minima at around $z \simeq 4.1$ Å and $z \simeq 15$ Å due to the boundary potentials applied to z,[41] a shallow free energy barrier of 2.0 kcal/mol is seen at around $z = 5.5$ Å;

beyond this point the PMF remains roughly constant. Thus, the UB state has a local minimum at around 4.5 Å, and moving further into the bulk water environment (e.g., $z \simeq 12$ Å) destabilizes the UB state by about 0.5 kcal/mol.

To calculate the free energy difference $\Delta G_{binding}^{PMF}$ (eq 4), the boundary of the DB state and the reference (z^*) of the UB state need to be defined. Although this is not straightforward, the result is largely insensitive to the precise choice of boundaries. From Figures 4a and 5a, we set $1.00 \leq z \leq 1.80$ Å to be the DB region and z^* to be 12.0 Å, respectively. The statistical error in $\Delta G_{binding}^{PMF}$ is estimated separately for the numerator (without the leading $\{C°\}^{1/3}$ factor) and denominator of eq 4 from the 2D and 1D metadynamics trajectories, respectively, and are illustrated in Figure 5b and c. The two results converge well at 100 and 40 ns, respectively; thus, the values thereafter are used to take the average and standard deviation; together with $C° = 1/1660$ Å⁻³, this gives the estimate of $\Delta G_{binding}^{PMF}$ with statistical uncertainty to be -11.9 ± 0.3 kcal/mol.

The effect of the tube constraint on the free energies ΔG_{tube}^{bd} and ΔG_{tube}^{unb} can also be estimated through numerical integrations. Since u_{tube} is effectively always zero for the DB state, $\Delta G_{tube}^{bd} = 0$. For the unbound state, eq 5 can be approximated as[59]

$$e^{-\beta \Delta G_{tube}^{unb}} = \{C°\}^{2/3} \int_0^{\infty} e^{-\beta u_{tube}(r)} 2\pi r \, dr \qquad (16)$$

This gives $\Delta G_{tube}^{unb} = 1.8$ kcal/mol. In other words, the metadynamics simulations lead to a site specific binding free energy $\Delta G_{binding}^{1,2}$ of -10.1 ± 0.3 kcal/mol.

Alchemical Free Energy Calculations. Next the binding free energy for the DB state is examined with alchemical FEP calculations. As described above, to ensure a smooth solvation change at the binding site as the bound HCOO⁻ decouples from the system, an intermediate structure is established in
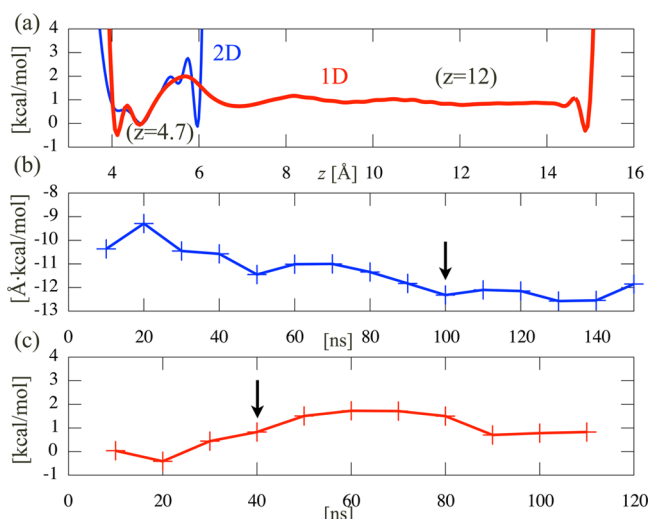
Figure 5. Potential of mean force (PMF) for longer range of z and convergence of estimated binding free energy from metadynamics. (a) The red curve is the 1D PMF from one-dimensional metadynamics simulations for $4.0 \leq z \leq 15.0$ (the wells near $z \sim 4$ and $z \sim 15$ are due to the boundary restraints in the metadynamics simulations); the blue curve is the long-range portion of the 1D PMF constructed by integrating the 2D PMF in Figure 3 over s. Note the difference in scale between Figure 4 and part a. (b, c) Time evolution of the estimated free energy of (b) the DB state and (c) the unbound state, using the PMF value at 4.7 Å as reference. Black arrows indicate where the PMFs are considered converged, and results thereafter are used to estimate the average and standard deviation of the computed binding free energy.

which two water molecules (W3 and W4) and HCOO⁻ are bound to Ti1 and Ti2 simultaneously, although they do not interact with each other (as illustrated in Figure 1). The results for the individual steps of the alchemical FEP calculations for the bound and unbound states are summarized in Figures 6 and 7, respectively. The general trends in those free energy components are largely within expectation; that is, those associated with annihilation of partial charges closely follow linear response,[44,60] while the contributions from restraining potentials and van der Waals interactions exhibit somewhat more complex dependence on the coupling parameter. The statistical uncertainties are fairly large when applying the harmonic restraints with small λ (between 0.0 and 0.1 in Figure 6(1) and 0.0 and 0.01 in Figure 7(1), respectively), although the standard deviations remain small (0.3 and 0.8 kcal/mol); taking even smaller λ steps does not change the result (not shown). Overall, the free energy changes $\Delta G_{uncouple}^{bd}$ and $\Delta G_{uncouple}^{unb}$ are evaluated to be 203.7 ± 0.5 and 200.8 ± 0.9 kcal/mol, respectively. The translational free energy contributions are calculated following eqs 13 and 15 with a box of the dimensions $28.9 \times 31.3 \times 66.3$ Å³ (box size along z is 90.93 Å and the thickness of the TiO₂ slab is 16.25 Å); since many terms in eqs 13 and 15 cancel, we get as a difference $\Delta\Delta G_{trans} = \Delta G_{trans}^{bd} - \Delta G_{trans}^{unb} = 5.6$ kcal/mol. Thus, the binding free energy $\Delta G_{binding}^{1,2}$ is calculated to be −8.5 ± 1.0 kcal/mol, in good agreement with the value of −10.1 ± 0.3 kcal/mol from metadynamics simulations.

Preliminary Binding/Unbinding Kinetics Analysis. Figures 8 and 9 show the distribution of configurations in the approximate transition state ensemble on the 2D PMF and the corresponding committor distributions, respectively. These results show that, while these approximate transition state
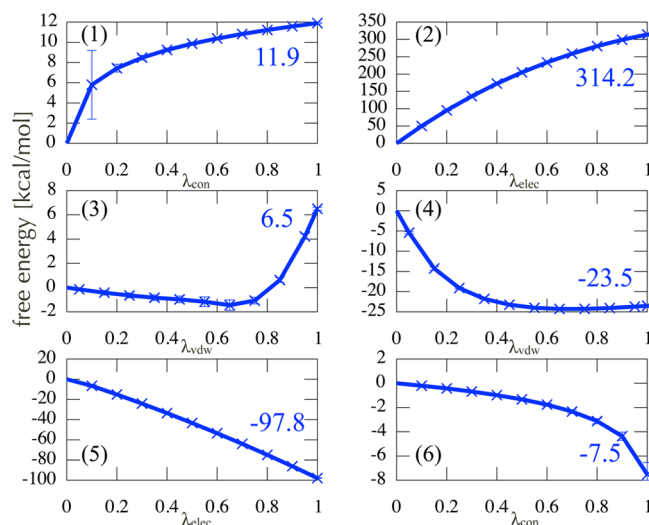

Figure 6. Accumulative free energy changes (i.e., $\int_0^\lambda d\lambda' (\partial G/\partial \lambda')$) for the six steps of alchemical transformation for the doubly bound state (see also Figure 1): (1) applying harmonic restraints to the H and O atoms in HCOO⁻, (2) charge removal from W1, W2, HCOO⁻, and Na⁺, (3) removal of vdW interactions from W1, W2 and insertion of chargeless W3, W4 above Ti1 and Ti2 via harmonic restraints, (4) removal of vdW interactions from HCOO⁻, (5) charging of W3 and W4, and (6) removal of harmonic restraints for W3 and W4. Error bars estimated with the BAR method are scaled by 10 for clarity (most are still too small to be visible), and the total error is obtained by the Gaussian error propagation of individual steps. Note that there are λ-independent positional restraints applied to the C in HCOO⁻, Na⁺, W1, and W2 throughout the alchemical FEP simulations; the effects of these restraints are evaluated analytically through ΔG_{trans}^{bd} (eq 13).
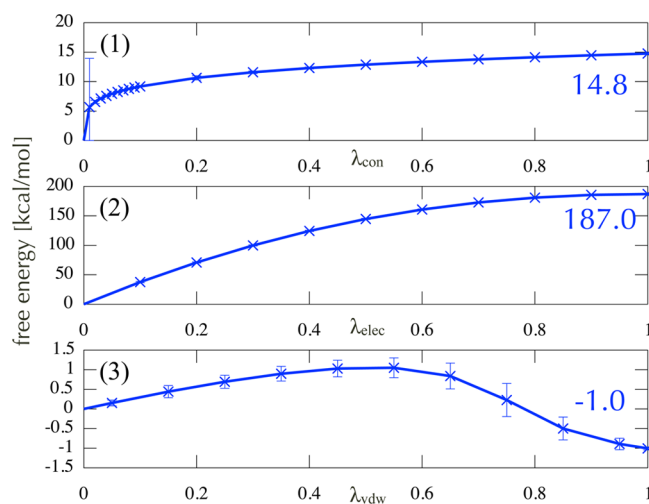

Figure 7. Accumulative free energy changes (i.e., $\int_0^\lambda d\lambda' (\partial G/\partial \lambda')$) for the three steps of alchemical transformation for the unbound state: (1) applying harmonic restraints to H and O atoms in HCOO⁻, (2) charge removal from HCOO⁻ and Na⁺, (3) removal of vdW interactions from HCOO⁻. Error bars estimated with the BAR method are scaled by 10 for clarity, and the total error is obtained by the Gaussian error propagation of individual steps. Note that there are λ-independent positional restraints applied to the C in HCOO⁻ and Na⁺ throughout the alchemical FEP simulations; the effects of these restraints are evaluated analytically through ΔG_{trans}^{ubd} (eq 15).

configurations have very similar s, z values in the saddle point region on the 2D PMF, the committor distributions are far from that expected for a true transition state ensemble; that is,
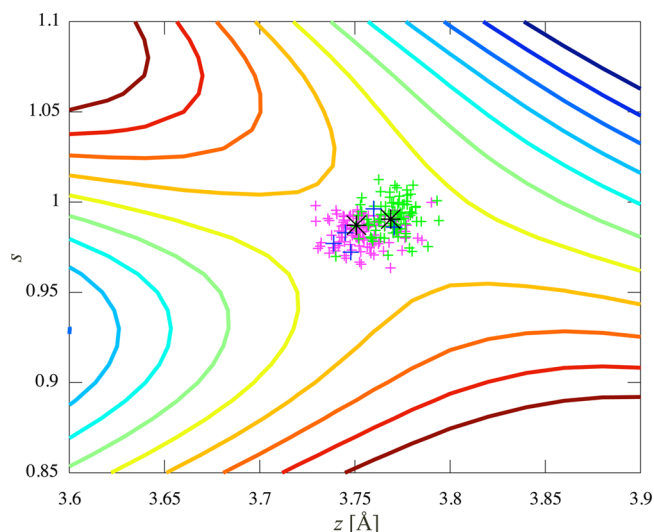
Figure 8. Distribution of the approximate transition state configurations (200) sampled around two reference points (marked with black stars, left: TS1 and right: TS2) on the 2D PMF, together with the free energy surface shown in contour lines (drawn every 0.5 kcal/mol). From each configuration, 100 NVE trajectories are carried out in both forward and backward directions ($\simeq 1$ ps in each direction) to compute the committor distribution (Figure 9). The color code of the configurations indicates the dominant fate of trajectories initiated from each configuration: magenta, SB−SB; light green, UB−UB; and blue, SB−UB or UB−SB.
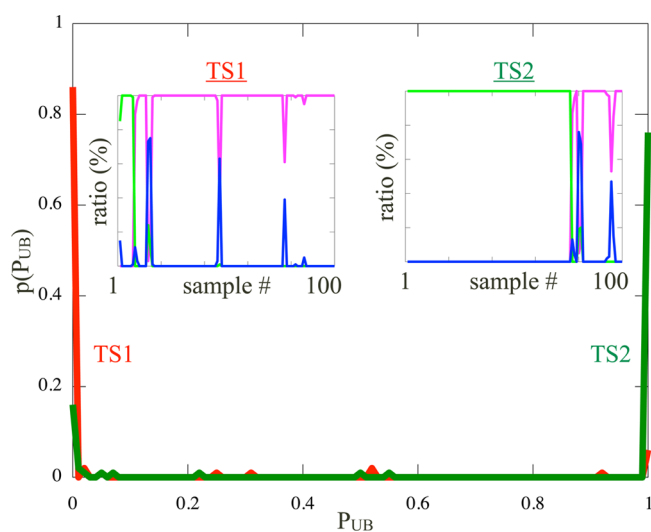

Figure 9. Committor distributions for the approximate transition state ensemble shown in Figure 8. Inset shows the actual percentage of the SB−SB (magenta), UB−UB (light green), and SB−UB or UB−SB (blue) trajectories for the collected configurations using TS1 and TS2 (black stars in Figure 8) as references.

rather than being peaked around the value of 0.5, the committor distributions for configurations collected with TS1 (TS2) as the reference peak around 0 (1). These results strongly suggest that to properly describe the binding/unbinding kinetics, additional coordinate(s) beyond s and z need to be explicitly included, further highlighting the complexity of the binding/unbinding process.

To clearly identify these "hidden" degree(s) of freedom as part of the reaction coordinate, one needs to carry out extensive sampling of unbiased transition events and systematically

analyze key variables that predict committor distributions.[56,61−64] This is beyond the scope of current work. Nevertheless, it is encouraging that several unbiased reactive trajectories have been harvested from our calculations (see inset of Figure 9) and these can be used to seed transition path sampling calculations[65] in the future.

As a preliminary analysis, we examine one such unbiased reactive trajectory, which is illustrated by the snapshots in Figure 10 and the time-evolution of key coordinates in Figure
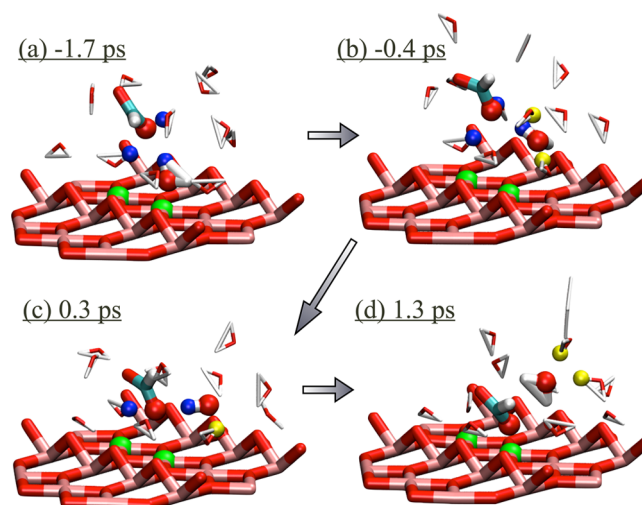

Figure 10. Snapshots from an unbiased reactive trajectory that describes the binding process. Time is relative to the approximate transition state configuration, and the trajectory is propagated both forward and backward in time for 10 ps. Only the solvent waters within 6 Å of the formate ion or the initially bound water (to be replaced by the formate ion) are shown, and blue and red spheres represent the hydrogen atoms within 2.1 Å of the key oxygen atoms in the formate ion and initially bound water (both shown by red spheres), respectively. Other coloring follows the scheme used in Figure 1

11. As also indicated by the 2D-PMF, prior to the binding of the formate ion, the water molecule that occupies the binding site needs to lift off the surface (Figure 10a →b); as the water desorbs, the water oxygen quickly (in a few hundreds femtoseconds, see Figure 11 bottom panel) form hydrogen bonds with surrounding water molecules (shown as yellow spheres in Figure 10). During the next 0.7 ps the formate anion approaches the Ti site, and the formate oxygen changes its hydrogen bonding partners (shown as blue spheres in Figure 10) in the process; the desorbed water molecule remains near both the formate anion and the surface Ti atom. Right after the 0.3 ps snapshot (Figure 10(c)), the Ti−O bond between the surface Ti atom and the formate anion is quickly formed (Figure 11 top panel); this is accompanied by the removal of all hydrogen bonds associated with the bound formate oxygen and full release of the desorbed water molecule into the bulk (Figure 10d). In short, this unbiased reactive trajectory hints at the importance of hydrogen bonding patterns associated with the adsorbate oxygen and the water molecule that originally occupies the binding site for describing the kinetics of the binding/unbinding process. This observation is in line with findings for other isomerization processes in solution[57] and proteins,[56,61,62] although quantitative insights require more extensive transition path sampling calculations.
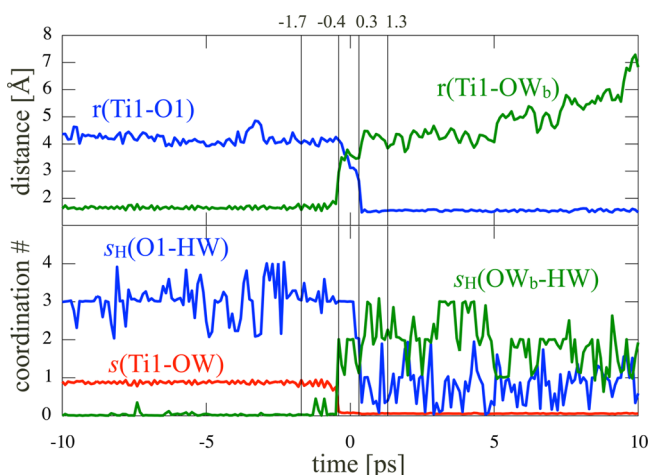
Figure 11. Time evolution of selected coordinates (top panel, distances between Ti and O1/OW_b; bottom panel, hydrogen coordination number around O1 and OW_b) in the unbiased reactive trajectory. O1 and OW_b are the adsorbing/desorbing oxygen atoms in the formate anion/water during the binding process, respectively, and Ti1 is the binding site. Hydrogen coordination numbers s_H(O1-HW) and s_H(OW_b-HW) are defined in using eq 9 with $d_0 = 1.80$ and $r_0 = 0.40$ Å. The oxygen coordination number around Ti1 (s(Ti1-OW)) is also shown for comparison.

CONCLUDING REMARKS

Molecular simulations hold great promise of providing physical insights into factors that dictate the binding of (bio)molecules to liquid/solid and liquid/NP interfaces. The quantitative reliability of such simulations depend on both the quality of the force field, which describes the underlying intermolecular interactions, and adequate sampling of configurations relevant to the binding process. Compared to the development of accurate and transferrable force fields,[26,66,67] the issue of adequate sampling has received somewhat less attention and most previous studies employed one-dimensional PMF simulations to characterize the binding process.

In the current work, using the example of formate anion binding to the rutile TiO_2 (110) surface, we illustrate the importance of explicitly considering the change of surface solvation during the binding process. In metadynamics simulations, the role of desolvation is examined by introducing the solvent coordination number of the binding site, s, as a collective variable in addition to the distance of the adsorbate orthogonal to the surface (z). The resulting two-dimensional potential of mean force clearly shows that explicitly including the local desolvation of the binding site on the TiO_2 surface has a major impact on the convergence and result of the binding free energy calculations. Furthermore, this desolvation process is somewhat uncoupled from the $HCOO^-$ binding coordinate (z), which suggests that the commonly used one-dimensional umbrella sampling protocol along z cannot sample the desolvation process effectively. Indeed, projecting the 2D PMF into a 1D-PMF along either z or s leads to large errors in the free energy barriers. This finding suggests the need to revisit previous potential of mean force calculations of peptide binding to TiO_2 surfaces in solution, carefully examining the role of desolvation, especially for the (un)binding kinetics. We also note that this issue is not expected to be a special case for the TiO_2/water interface but can be important to any strongly charged/ionic surfaces in solution, where desolvation is likely a rare event but necessary for binding of other charged

(bio)molecules; whether the same issue applies to binding at soft interfaces such as the water-membrane interface[68,69] is also interesting to investigate.

The binding affinity of the formate anion in the doubly bound state is also calculated using an alchemical free energy perturbation approach, in which the solvation state of the binding site is also carefully considered by explicitly introducing water molecules to the binding site as the adsorbate is decoupled from the system. The results from metadynamics and alchemical FEP simulations are consistent and therefore reinforce the convergence of these calculations. With the specific force field used here, we estimate that $HCOO^-$ binds strongly (to a specific site, see eq 1) to the rutile TiO_2 (110) surface with an affinity of ~7 kcal/mol. These estimates are substantially larger than those reported in previous simulations;[25] although part of the difference is due to the use of different force fields, the analysis here suggests that previous results are likely influenced by sampling problems. The strong binding found here also appears to be contradictory with the experimental suggestions[14,31,70] that the rutile TiO_2 (110) surface favors the binding of cationic species over anionic ones. However, we note that a neutral surface (i.e., no OH^- group on the surface) is used here, while some suggested that a negatively charged surface is more realistic;[27,30,71] for example, TiO_2 bound water has substantially reduced pK_a[72,73] and the point of zero charge of TiO_2 is around 5.[74] Therefore, in addition to systematically examining the quality of the force field, care has to be exercised to treat the ionization state of surface water molecules under specific solution conditions. One possibility is to employ a constant pH formulation[75] in which the ionization state of surface water adjusts on the fly; once the titration state distribution is equilibrated, the configuration can be used in subsequent binding free energy simulations. Above all, quantitative experimental studies of small molecule binding to TiO_2 surfaces are required to aid the development of robust computational models that can be used to probe in detail more complex interfaces.

Finally, our preliminary committor analysis for the approximate transition state ensemble constructed based on the 2D-PMF further highlights the complexity of the microscopic binding/unbinding process. The computed committor distributions clearly indicate that while s and z coordinates serve as good order parameters, additional coordinate(s) are required to properly describe the binding/unbinding kinetics. Examination of one unbiased reactive trajectory hints at the importance of hydrogen bonding patterns associated with the adsorbate and desorbing water molecule, although quantitative insights require a more systematic analysis of the reactive trajectories using transition path sampling.

ASSOCIATED CONTENT

Ⓢ Supporting Information
Charge parameters of the formate anion and TiO_2 atoms used in the current simulation. This material is available free of charge via the Internet at http://pubs.acs.org/.

AUTHOR INFORMATION

Corresponding Author
*E-mail: cui@chem.wisc.edu.

Notes
The authors declare no competing financial interest.

■ REFERENCES

(1) Allen, T. M.; Cullis, P. R. Drug Delivery Systems: Entering the Mainstream. *Science* **2004**, *303*, 1818−1822.

(2) Oberdörster, G.; Oberdörster, E.; Oberdörster, J. Nanotoxicology: An Emerging Discipline Evolving from Studies of Ultrafine Particles. *Environ. Health Perspect.* **2005**, *113*, 823−839.

(3) Nel, A.; Xia, T.; Mädler, L.; Li, N. Toxic Potential of Materials at the Nanolevel. *Science* **2006**, *311*, 622−627.

(4) Leroueil, P. R.; Hong, S.; Mecke, A.; Baker, J. R.; Orr, B. G.; Banaszak Holl, M. M. Nanoparticle Interaction with Biological Membranes: Does Nanotechnology Present a Janus Face? *Acc. Chem. Res.* **2007**, *40*, 335−342.

(5) Fei, L.; Perrett, S. Effect of Nanoparticles on Protein Folding and Fibrillogenesis. *Int J Mol Sci* **2009**, *10*, 646−655.

(6) Lundqvist, M.; Sethson, I.; Jonsson, B.-H. Protein Adsorption onto Silica Nanoparticles: Conformational Changes Depend on the Particles' Curvature and the Protein Stability. *Langmuir* **2004**, *20*, 10639−10647.

(7) Zhou, H. S.; Aoki, S.; Honma, I.; Hirasawa, M.; Nagamune, T.; Komiyama, H. Conformational Change of Protein Cytochrome b-562 Adsorbed on Colloidal Gold Particles; Absorption Band Shift. *Chem. Commun.* **1997**, 605−606.

(8) Schravendijk, P.; Ghiringhelli, L. M.; Site, L. D.; van der Vegt, N. F. Interaction of Hydrated Amino Acids with Metal Surfaces: A Multiscale Modeling Description. *J. Phys. Chem. C* **2007**, *111*, 2631−2642.

(9) Ghiringhelli, L. M.; Hess, B.; van der Vegt, N. F. A.; Delle Site, L. Competing Adsorption between Hydrated Peptides and Water onto Metal Surfaces: From Electronic to Conformational Properties. *J. Am. Chem. Soc.* **2008**, *130*, 13460−13464.

(10) Di Felice, R.; Corni, S. Simulation of Peptide Surface Recognition. *J. Phys. Chem. Lett.* **2011**, *2*, 1510−1519.

(11) Lower, B. H.; Lins, R. D.; Oestreicher, Z.; Straatsma, T. P.; Hochella, M. F.; Shi, L.; Lower, S. K. In Vitro Evolution of a Peptide with a Hematite Binding Motif That May Constitute a Natural Metal-Oxide Binding Archetype. *Environ. Sci. Technol.* **2008**, *42*, 3821−3827.

(12) Goede, K.; Busch, P.; Grundmann, M. Binding Specificity of a Peptide on Semiconductor Surfaces. *Nano Lett.* **2004**, *4*, 2115−2120.

(13) Naik, R. R.; Brott, L. L.; Clarson, S. J.; Stone, M. O. Silica-Precipitating Peptides Isolated from a Combinatorial Phage Display Peptide Library. *J. Nanosci. Nanotechnol.* **2002**, *2*, 95−100.

(14) Hayashi, T.; Sano, K.-I.; Shiba, K.; Kumashiro, Y.; Iwahori, K.; Yamashita, I.; Hara, M. Mechanism Underlying Specificity of Proteins Targeting Inorganic Materials. *Nano Lett.* **2006**, *6*, 515−519.

(15) Imamura, K.; Kawasaki, Y.; Nagayasu, T.; Sakiyama, T.; Nakanishi, K. Adsorption Characteristics of Oligopeptides Composed of Acidic and Basic Amino Acids on Titanium Surface. *J. Biosci. Bioeng.* **2007**, *103*, 7−12.

(16) Sano, K.-I.; Shiba, K. A Hexapeptide Motif that Electrostatically Binds to the Surface of Titanium. *J. Am. Chem. Soc.* **2003**, *125*, 14234−14235.

(17) Shiba, K. Exploitation of Peptide Motif Sequences and Their Use in Nanobiotechnology. *Curr. Opin. Biotechnol.* **2010**, *21*, 412−425.

(18) Diebold, U. The Surface Science of Titanium Dioxide. *Surf. Sci. Rep.* **2003**, *48*, 53−229.

(19) Chen, H. H.; Nanayakkara, C. E.; Grassian, V. H. Titanium Dioxide Photocatalysis in Atmospheric Chemistry. *Chem. Rev.* **2012**, *112*, 5919−5948.

(20) Rubasinghege, G.; Grassian, V. H. Role(s) of Adsorbed Water in the Surface Chemistry of Environmental Interfaces. *Chem. Commun.* **2013**, *49*, 3071−3094.

(21) Takemoto, S.; Hattori, M.; Yoshinari, M.; Kawada, E.; Oda, Y. Corrosion Behavior and Surface Characterization of Titanium in Solution Containing Fluoride and Albumin. *Biomaterials* **2005**, *26*, 829−837.

(22) Aziz-Kerrzo, M.; Conroy, K. G.; Fenelon, A. M.; Farrell, S. T.; Breslin, C. B. Electrochemical Studies on the Stability and Corrosion Resistance of Titanium-Based Implant Materials. *Biomaterials* **2001**, *22*, 1531−1539.

(23) Dickerson, M. B.; Jones, S. E.; Cai, Y.; Ahmad, G.; Naik, R. R.; Kröger, N.; Sandhage, K. H. Identification and Design of Peptides for the Rapid, High-Yield Formation of Nanoparticulate TiO_2 from Aqueous Solutions at Room Temperature. *Chem. Mater.* **2008**, *20*, 1578−1584.

(24) Chen, H.; Su, X.; Neoh, K.-G.; Choe, W.-S. QCM-D Analysis of Binding Mechanism of Phage Particles Displaying a Constrained Heptapeptide with Specific affinity to SiO_2 and TiO_2. *Anal. Chem.* **2006**, *78*, 4872−4879.

(25) Monti, S.; Walsh, T. R. Free Energy Calculations of the Adsorption of Amino Acid Analogues at the Aqueous Titania Interface. *J. Phys. Chem. C* **2010**, *114*, 22197−22206.

(26) Schneider, J.; Ciacchi, L. C. A Classical Potential to Model the Adsorption of Biological Molecules on Oxidized Titanium Surfaces. *J. Chem. Theo. Comp.* **2011**, *7*, 473−484.

(27) Schneider, J.; Colombi Ciacchi, L. Specific Material Recognition by Small Peptides Mediated by the Interfacial Solvent Structure. *J. Am. Chem. Soc.* **2012**, *134*, 2407−2413.

(28) Li, C.; Monti, S.; Carravetta, V. Journey toward the Surface: How Glycine Adsorbs on Titania in Water Solution. *J. Phys. Chem. C* **2012**, *116*, 18318−18326.

(29) Monti, S.; van Duin, A. C. T.; Kim, S.-Y.; Barone, V. Exploration of the Conformational and Reactive Dynamics of Glycine and Diglycine on TiO_2: Computational Investigations in the Gas Phase and in Solution. *J. Phys. Chem. C* **2012**, *116*, 5141−5150.

(30) Wu, C.; Skelton, A. A.; Chen, M.; Vlček, L.; Cummings, P. T. Modeling the Interaction between Integrin−Binding Peptide (RGD) and Rutile Surface: The Effect of Na^+ on Peptide Adsorption. *J. Phys. Chem. C* **2011**, *115*, 22375−22386.

(31) Hayashi, T.; Sano, K.-I.; Shiba, K.; Iwahori, K.; Yamashita, I.; Hara, M. Critical Amino Acid Residues for the Specific Binding of the Ti-Recognizing Recombinant Ferritin with Oxide Surfaces of Titanium and Silicon. *Langmuir* **2009**, *25*, 10901−10906.

(32) Carravetta, V.; Monti, S. Peptide−TiO_2 Surface Interaction in Solution by Ab Initio and Molecular Dynamics Simulations. *J. Phys. Chem. B* **2006**, *110*, 6160−6169.

(33) Harding, J. H.; Duffy, D. M.; Sushko, M. L.; Rodger, P. M.; Quigley, D.; Elliott, J. A. Computational Techniques at the Organic−Inorganic Interface in Biomineralization. *Chem. Rev.* **2008**, *108*, 4823−4854.

(34) Schneider, J.; Ciacchi, L. C. First Principles and Classical Modeling of the Oxidized Titanium (0001) Surface. *Surf. Sci.* **2010**, *604*, 1105−1115.

(35) Jorgensen, W. L.; Chandrasekhar, J.; Madura, J. D.; Impey, R. W.; Klein, M. L. Comparison of Simple Potential Functions for Simulating Liquid Water. *J. Chem. Phys.* **1983**, *79*, 926−935.

(36) Jakalian, A.; Bush, B. L.; Jack, D. B.; Bayly, C. I. Fast, Efficient Generation of High-Quality Atomic Charges. AM1-BCC Model: I. Method. *J. Comput. Chem.* **2000**, *21*, 132−146.

(37) Jakalian, A.; Jack, D. B.; Bayly, C. I. Fast, Efficient Generation of High-Quality Atomic Charges. AM1-BCC Model: II. Parameterization and Validation. *J. Comput. Chem.* **2002**, *23*, 1623−1641.

(38) Essmann, U.; Perera, L.; Berkowitz, M. L.; Darden, T.; Lee, H.; Pedersen, L. G. A Smooth Particle Mesh Ewald Method. *J. Chem. Phys.* **1995**, *103*, 8577−8593.

(39) Ryckaert, J.-P.; Ciccotti, G.; Berendsen, H. J. C. Numerical Integration of the Cartesian Equations of Motion of a System with Constraints: Molecular Dynamics of n-Alkanes. *J. Comput. Phys.* **1977**, *23*, 327−341.

(40) Case, D. A. et al. *AMBER 12*; University of California: San Francisco, 2012,

(41) Bonomi, M.; Branduardi, D.; Bussi, G.; Camilloni, C.; Provasi, D.; Raiteri, P.; Donadio, D.; Marinelli, F.; Pietrucci, F.; Broglia, R. A.; Parrinello, M. PLUMED: A Portable Plugin for Free-Energy Calculations with Molecular Dynamics. *Comput. Phys. Commun.* **2009**, *180*, 1961−1972.

(42) Gilson, M. K.; Given, J. A.; Bush, B. L.; McCammon, J. A. The Statistical-Thermodynamic Basis for Computation of Binding Affinities: A Critical Review. *Biophys. J.* **1997**, *72*, 1047−1069.

(43) Deng, Y.; Roux, B. Calculation of Standard Binding Free Energies: Aromatic Molecules in the T4 Lysozyme L99A Mutant. *J. Chem. Theo. Comp.* **2006**, *2*, 1255−1273.

(44) Woo, H.-J.; Roux, B. Calculation of Absolute Protein−Ligand Binding Free Energy from Computer Simulations. *Proc. Natl. Acad. Sci. U.S.A.* **2005**, *102*, 6825−6830.

(45) Hill, T. L. *An Introduction to Statistical Thermodynamics*; Dover Publications: New York, 1986.

(46) Laio, A.; Parrinello, M. Escaping Free-Energy Minima. *Proc. Natl. Acad. Sci. U.S.A.* **2002**, *99*, 12562−12566.

(47) Pohorille, A.; Jarzynski, C.; Chipot, C. Good Practices in Free-Energy Calculations. *J. Phys. Chem. B* **2010**, *114*, 10235−10253.

(48) Laio, A.; Gervasio, F. L. Metadynamics: A Method to Simulate Rare Events and Reconstruct the Free Energy in Biophysics, Chemistry, and Material Science. *Rep. Prog. Phys.* **2008**, *71*, 126601.

(49) Barducci, A.; Bussi, G.; Parrinello, M. Well-Tempered Metadynamics: A Smoothly Converging and Tunable Free-Energy Method. *Phys. Rev. Lett.* **2008**, *100*, 020603.

(50) Hünenberger, P. H.; McCammon, J. A. Ewald Artifacts in Computer Simulations of Ionic Solvation and Ion−Ion Interaction: A Continuum Electrostatics Study. *J. Chem. Phys.* **1999**, *110*, 1856.

(51) Kastenholz, M. A.; Hünenberger, P. H. Computation of Methodology-Independent Ionic Solvation Free Energies from Molecular Simulations. I. The Electrostatic Potential in Molecular Liquids. *J. Chem. Phys.* **2006**, *124*, 124106.

(52) Lu, X.; Cui, Q. Charging Free Energy Calculations Using the Generalized Solvent Boundary Potential (GSBP) and Periodic Boundary Condition: A Comparative Analysis Using Ion Solvation and Reduction Potential in Proteins. *J. Phys. Chem. B* **2013**, *117*, 2005−2018.

(53) Beutler, T. C.; Mark, A. E.; van Schaik, R. C.; Gerber, P. R.; van Gunsteren, W. F. Avoiding Singularities and Numerical Instabilities in Free Energy Calculations Based on Molecular Simulations. *Chem. Phys. Lett.* **1994**, *222*, 529−539.

(54) Zacharias, M.; Straatsma, T. P.; McCammon, J. A. Separation-Shifted Scaling, a New Scaling Method for Lennard-Jones Interactions in Thermodynamic Integration. *J. Chem. Phys.* **1994**, *100*, 9025.

(55) Bennett, C. H. Efficient Estimation of Free Energy Differences from Monte Carlo Data. *J. Comput. Phys.* **1976**, *22*, 245−268.

(56) Bolhuis, P.; Dellago, C.; Chandler, D. Reaction Coordinates of Biomolecular Isomerization. *Proc. Natl. Acad. Sci. U.S.A.* **2000**, *97*, 5877−5882.

(57) Geissler, P. L.; Dellago, C.; Chandler, D. Kinetic Pathways of Ion Pair Dissociation in Water. *J. Phys. Chem. B* **1999**, *103*, 3706−3710.

(58) Bolhuis, P. G. Kinetic Pathways of β-Hairpin (Un)folding in Explicit Solvent. *Biophys. J.* **2005**, *88*, 50−61.

(59) Allen, T. W.; Andersen, O. S.; Roux, B. Energetics of ion conduction through the gramicidin channel. *Proc. Natl. Acad. Sci. U.S.A.* **2004**, *101*, 117−122.

(60) Levy, R. M.; Belhadj, M.; Kitchen, D. B. Gaussian Fluctuation Formula for Electrostatic Free Energy Changes. *J. Chem. Phys.* **1991**, *95*, 3627−3633.

(61) Ma, A.; Dinner, A. R. Automatic Method for Identifying Reaction Coordinates in Complex Systems. *J. Phys. Chem. B* **2005**, *109*, 6769−6779.

(62) Qi, B.; Muff, S.; Caflisch, A.; Dinner, A. R. Extracting Physically Intuitive Reaction Coordinates from Transition Networks of a β-Sheet Miniprotein. *J. Phys. Chem. B* **2010**, *114*, 6979−6989.

(63) Best, R. B.; Hummer, G. Reaction coordinates and rates from transition paths. *Proc. Natl. Acad. Sci. U.S.A.* **2005**, *102*, 6732−6737.

(64) Ma, L.; Cui, Q. Activation mechanism of a signaling protein at atomic resolution from advanced computations. *J. Am. Chem. Soc.* **2007**, *129*, 10261−10268.

(65) Dellago, C.; Bolhuis, P. G.; Geissler, P. L. *Advances in Chemical Physics*; John Wiley & Sons, Inc.: Hoboken, NJ, 2003; pp 1−78.

(66) Freeman, C. L.; Harding, J. H.; Cooke, D. J.; Elliott, J. A.; Lardge, J. S.; Duffy, D. M. New Forcefields for Modeling Biomineralization Processes. *J. Phys. Chem. C* **2007**, *111*, 11943−11951.

(67) Nakamura, H.; Ohto, T.; Nagata, Y. Polarizable Site Charge Model at Liquid/Solid Interfaces for Describing Surface Polarity: Application to Structure and Molecular Dynamics of Water/Rutile TiO_2 (110) Interface. *J. Chem. Theo. Comp.* **2013**, 1193−1201.

(68) Neale, C.; Bennett, W. F. D.; Tieleman, D. P.; Pomes, R. Statistical Convergence of Equilibrium Properties in Simulations of Molecular Solutes Embedded in Lipid Bilayers. *J. Chem. Theo. Comp.* **2011**, *7*, 4175−4188.

(69) Yoo, J.; Cui, Q. Chemical vs. Mechanical Perturbations on the Protonation State of Arginine in Complex Lipid Membranes: Insights from Microscopic pK_a Calculations. *Biophys. J.* **2010**, *99*, 1529−1538.

(70) Gertler, G.; Fleminger, G.; Rapaport, H. Characterizing the Adsorption of Peptides to TiO_2 in Aqueous Solutions by Liquid Chromatography. *Langmuir* **2010**, *26*, 6457−6463.

(71) Předota, M.; Bandura, A. V.; Cummings, P. T.; Kubicki, J. D.; Wesolowski, D. J.; Chialvo, A. A.; Machesky, M. L. Electric Double Layer at the Rutile (110) Surface. 1. Structure of Surfaces and Interfacial Water from Molecular Dynamics by Use of Ab Initio Potentials. *J. Phys. Chem. B* **2004**, *108*, 12049−12060.

(72) Cheng, J.; Sprik, M. Acidity of the Aqueous Rutile TiO_2 (110) Surface from Density Functional Theory Based Molecular Dynamics. *J. Chem. Theo. Comp* **2010**, *6*, 880−889.

(73) Gaigeot, M.-P.; Sprik, M.; Sulpizi, M. Oxide/Water Interfaces: How the Surface Chemistry Modifies Interfacial Water Properties. *J. Phys.: Condens. Matter* **2012**, *24*, 124106.

(74) Ridley, M. K.; Machesky, M. L.; Palmer, D. A.; Wesolowski, D. J. Potentiometric Studies of the Rutile−Water Interface: Hydrogen-Electrode Concentration-Cell Versus Glass-Electrode Titrations. *J. Colloids Surf. A: Physicochem. Eng. Aspects* **2002**, *204*, 295−308.

(75) Donnini, S.; Tegeler, F.; Groenhof, G.; Grubmuller, H. Constant pH Molecular Dynamics in Explicit Solvent with λ-Dynamics. *J. Chem. Theo. Comp.* **2011**, *7*, 1962−1978.